

Long-range interactions in Weyl photonic crystals

Lei Ying,¹ Ming Zhou,¹ Michael Mattei,² Boyuan Liu,¹ Paul Campagnola,³ Randall H. Goldsmith,² and Zongfu Yu^{1,*}

¹Department of Electrical and Computer Engineering,
University of Wisconsin, Madison, Wisconsin 53706, USA

²Department of Chemistry, University of Wisconsin, Madison, Wisconsin 53706, USA

³Department of Biomedical Engineering, University of Wisconsin, Madison, Wisconsin 53706, USA

(Dated: December 16, 2024)

The interaction between quantum two-level systems is typically short-range in free space and most photonic environments. Here we show that Weyl photonic crystals can create significantly extended long-range interaction between distant quantum systems because of their diminishing momentum isosurfaces with equal frequencies around isolated Weyl points. The extended range of interaction is robust and does not rely on specific location or orientation of the transition dipoles. A general relation between the interaction range and properties of the isosurface is described, which provides a recipe to identify other photonic environments for that enable long-range interaction. This work lays the foundation to use Weyl photonic crystals as a platform to mediate quantum behavior.

The dipole-dipole interaction between two quantum two-level systems (TLS) is typically short-range. There has been strong interest in realizing long-range interactions to exploit collective physics such as superradiance [1, 2], collective frequency shift [3], Förster resonance energy transfer [4, 5], and quantum entanglement [6–12]. The ability to modulate the distance dependence of these processes could have potential applications in quantum information processing [8, 13] and energy conversion [14]. Two components contribute to the interaction: the evanescent near fields and the propagating far fields (Fig. 1a & b). To enable long-range interaction from the evanescent fields, one could use evanescent fields with a long tail. Kimble et al. showed that this scenario is possible for modes in the photonic bandgap but close to the band edge [15–17]. However, it is less obvious how to engineer propagating far fields to enable long-range interaction. It is the goal of this letter to provide a new perspective to understand the general physical mechanism that is responsible for long-range interaction induced by propagating far fields, and identify a specific structure, a Weyl photonic crystal, that is capable of extending that interaction range.

In free space, the range of far fields induced interaction is limited to the wavelength scale. When the wavelength is long, such as those in index-near-zero materials [18–20], the interaction range can increase proportionally. However, there are a few intriguing examples where the interaction range extends far beyond the effective wavelength. These include low-dimensional spaces, such as waveguides and fibers [2, 21, 22], or hyperbolic materials in selected directions [23–25]. These interesting but isolated examples heavily rely on very specific configurations. Thus, it is difficult to generalize the theoretical treatments to identify the underlying physics, which unfortunately remains elusive. In this letter, we show the deep connection between the long-range interaction and the size and shape of the iso-frequency surface in momentum space. It can be gener-

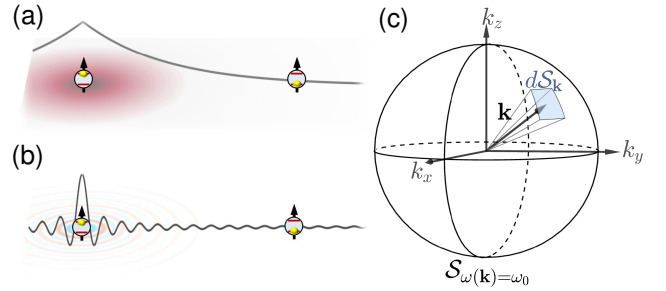


Figure 1. Schematics of interactions between two TLSs connected by (a) evanescent near-field modes, (b) propagating far-field modes (c) Isosurface $S_{\omega(\mathbf{k})=\omega_0}$ in momentum space, where $dS_{\mathbf{k}}$ is a small surface element.

alized to a broad range of physical systems and to identify new systems capable of realizing long-range interaction. As an example, we show the robust long-range interaction in a Weyl photonic crystal. Such a long-range interaction is realized not just along a single axis, but in 3D space for all directions with an interaction range far beyond the free space and effective wavelength.

We begin by examining the interaction between two TLSs over a long distance. The TLSs are embedded in a photonic environment that can be described by a dispersion relation $\omega = \omega(\mathbf{k})$. Using the example of free space, $\omega = c|\mathbf{k}| = ck$, where c is the light of speed. Other dispersion relations can be seen in metamaterials, photonic crystals or waveguides. The Hamiltonian of the TLSs and the photonic modes is given by [26]

$$\mathcal{H} = \sum_{i=1,2} \omega_0 \hat{\sigma}_i^+ \hat{\sigma}_i + \sum_{\mathbf{k}, \eta} \omega_{\mathbf{k}} \hat{a}_{\mathbf{k}, \eta}^+ \hat{a}_{\mathbf{k}, \eta} + i \sum_{i=1,2} \sum_{\mathbf{k}, \eta} g_{\mathbf{k}}(\mathbf{r}_i) \left(\hat{a}_{\mathbf{k}, \eta} \hat{\sigma}_i^+ e^{i\mathbf{k} \cdot \mathbf{r}_i} - \hat{a}_{\mathbf{k}, \eta}^+ \hat{\sigma}_i e^{-i\mathbf{k} \cdot \mathbf{r}_i} \right), \quad (1)$$

where ω_0 is the resonant transition frequency of the TLS. $\hat{\sigma}_i^{\pm}$ ($\hat{\sigma}_i$) is the raising (lowering) operator of i th TLS.

$\omega_{\mathbf{k}}$ and $\hat{a}_{\mathbf{k},\eta}^\dagger$ ($\hat{a}_{\mathbf{k},\eta}$) are the frequency and creation (annihilation) operator of photons, respectively. $g_{\mathbf{k},\eta}(\mathbf{r}_i) = \sqrt{\omega_{\mathbf{k}}/2\epsilon_0 V} \boldsymbol{\mu}_i \cdot \boldsymbol{\epsilon}_{\mathbf{k},\eta}$ is the coupling between the i th TLS and the photonic mode \mathbf{k} . Here, $\boldsymbol{\mu}_i$ is the transition dipole moment of the i th TLS and $\boldsymbol{\epsilon}_{\mathbf{k},\eta}$ is the polarization direction of the photonic mode \mathbf{k} and index η . One can derive the radiative interaction $\Gamma = \Gamma_{\text{Re}} + i\Gamma_{\text{Im}}$ between two TLSs based on the above Hamiltonian. The real and imaginary parts describe the cooperative decay rate and cooperative energy shift, respectively. The focus of this letter will be cooperative decay rate. Similar conclusions can be drawn for the cooperative energy shift.

We first provide a graphic illustration of why the interaction between TLSs is short-range in free space. Unlike most theoretical treatments used in the literature [24], we do not use Green functions to describe the radiative environment. Instead, we try to keep all radiative modes in their explicit forms in order to gain a more intuitive picture. As shown in Section I of supplementary material, the interaction between TLSs can be expressed in the following form:

$$\Gamma_{\text{Re}} = \iint_{S_{\omega_0(\mathbf{k})}} \rho_{\mathbf{k}} e^{i\mathbf{k}\cdot\mathbf{R}} dS_{\mathbf{k}}. \quad (2)$$

The integral is performed on an iso-surface in momentum space, i.e. all wavevectors \mathbf{k} that satisfy $\omega(\mathbf{k}) = \omega_0$. The integrand includes two terms. The first term is simply a polarization factor $\rho_{\mathbf{k}} = \frac{\omega_0}{16\epsilon_0\pi^2 v_g(\mathbf{k})} (\boldsymbol{\mu}_1 \cdot \boldsymbol{\epsilon}_{\mathbf{k}})(\boldsymbol{\mu}_2 \cdot \boldsymbol{\epsilon}_{\mathbf{k},\eta})^*$, which describes the relative orientation of the transition dipole $\boldsymbol{\mu}$ and the polarization of the electric field $\boldsymbol{\epsilon}$. Here v_g is the group velocity. For degenerate polarization states, the integration should also include all polarizations. Since the polarization factor $\rho_{\mathbf{k}}$ is independent of the inter-TLS distance, it does not affect the interaction range. It is the second term $e^{i\mathbf{k}\cdot\mathbf{R}}$ that plays the critical role in the physics of the interaction range. Here $\mathbf{R} = \mathbf{r}_1 - \mathbf{r}_2$ is the distance vector between the two TLSs. The integrand $\rho_{\mathbf{k}} e^{i\mathbf{k}\cdot\mathbf{R}}$ is a fast oscillating function, which generally results in cancellation of the integration when R is large. Therefore, the interaction is always short-range. We can see this effect in Fig. 2a. Here we consider two TLSs in free space. The spherical isosurface has a radius of $k = |\mathbf{k}| = \omega_0/c$. The real part of $\rho_{\mathbf{k}} e^{i\mathbf{k}\cdot\mathbf{R}}$ is plotted on the isosurface. When $R = 10\lambda$, there are rapid oscillations as \mathbf{k} varies on the isosurface. The resulting value of the integral is small, and therefore the interaction is weak at this long distance. Only when the inter-TLS distance is small, for example $R = 0.3\lambda$, the slow oscillation, as shown in Fig. 2c, can lead to a sizable value of integral and thus a strong interaction. The interaction decays as the distance R grows (Fig. 2d).

We now use the same graphic illustration to introduce an important observation: *the interaction range is*

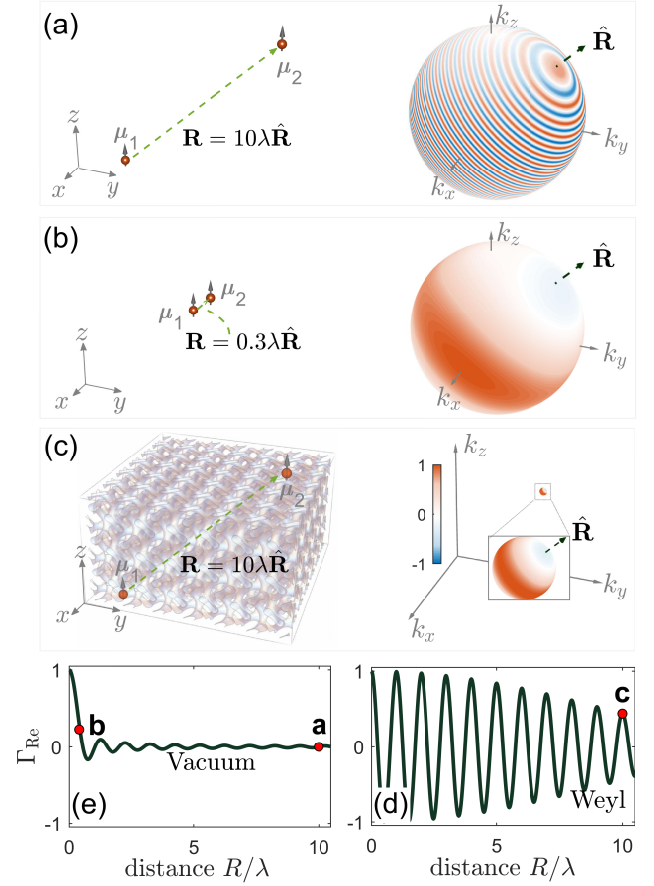


Figure 2. (a) Two dipolar quantum transitions spaced by a distance $R = 10\lambda$ in free space. The right panel shows the isosurface for the transition frequency in momentum space. The real part of integrand $\rho_{\mathbf{k}} e^{i\mathbf{k}\cdot\mathbf{R}}$ is plotted on the isosurface. Red and blue colors indicate positive and negative maximum, respectively. A long R leads to fast oscillation and cancellation of the integral over the isosurface. (b) Similar to (a) but with a shorter distance $R = 0.3\lambda$ and thus slow oscillation on the isosurface. (c) The situation can change significantly if two quantum transitions are placed in a general photonic environment, such as Weyl photonic crystal, where the isosurface can be very small. Here $R = 10\lambda$. The isosurface has a radius of $q = |\mathbf{k} - \mathbf{k}_c|$. The inset in the right panel shows the zoom-in view of the small isosurface, showing that even a large R may not result significant cancellation due to small isosurface size. $\hat{\mathbf{R}}$ in (a-c) is fixed as $(1, 0, 1)/\sqrt{2}$. (d) & (e) The real part of radiative interaction as a function of distance between two TLSs in free space and the Weyl photonic crystal, respectively. Red dots correspond to the cases in (a), (b), and (c), respectively.

inversely proportional to the size of the isosurface in momentum space. A large inter-TLS distance R on a large isosurface leads to a fast oscillating integrand on the isosurface that results in a small value of the integral. One way to counter this effect is to substantially reduce the isosurface size. Small isosurfaces can save the integral from cancellation even for a fast-oscillating func-

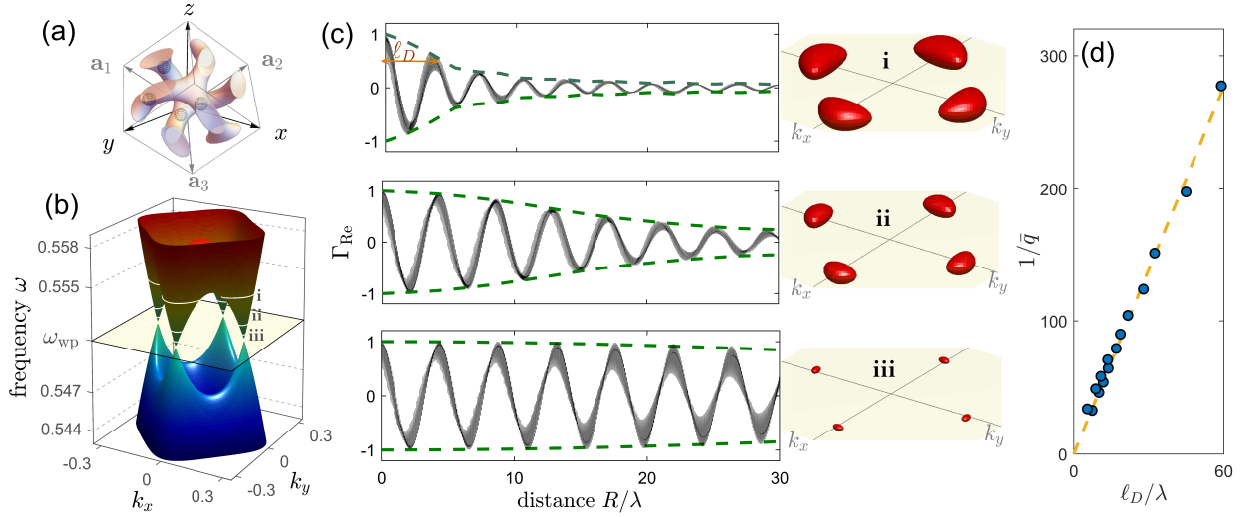


Figure 3. (a) Structure of Weyl photonic crystal. Double-gyroid dielectric structure in a body-centered cubic unit cell with a set of basis vectors $\mathbf{a}_1 = (-1/2, 1/2, 1/2)a$, $\mathbf{a}_2 = (1/2, -1/2, 1/2)a$, and $\mathbf{a}_3 = (1/2, 1/2, -1/2)a$, where a is the lattice constant. Four air spheres with a radius $r = 0.07a$ are located at $(1/4, -1/8, 1/2)a$, $(1/4, 1/8, 0)a$, $(5/8, 0, 1/4)a$ and $(3/8, 1/2, 1/4)a$, respectively. (b) Dispersion relation on the $k_z = 0$ plane. Three frequencies i, ii, iii are marked with white lines, to be discussed in (c). (c) The interaction strength Γ_{Re} as a function of distance for TLS transition frequencies (upper) $\omega = 0.5545$, (middle) 0.5520 and (lower) $0.5512c/a$, which correspond to the frequency i, ii, and iii in (b), respectively. The inter-TLS direction is $\hat{\mathbf{R}} = (-1, 1, 1)/\sqrt{3}$. The dipole orientations are $\hat{\boldsymbol{\mu}}_{1,2} = (-1, 1, 1)/\sqrt{3}$ and $\boldsymbol{\mu}_1$ is fixed at central point of the unit cell. Green dashed curves are the envelopes of the curve. Inset (i-iii) are the isosurfaces in momentum space. (d) The linear relationship between decay length ℓ_D and inverse size of isosurfaces $1/\bar{q}$.

tion. Figure 2c shows the integrand $\rho_{\mathbf{k}}e^{i\mathbf{k}\cdot\mathbf{R}}$ with a long inter-TLS distance $R = 10\lambda$ on an isosurface that has a radius that is 0.03 times that of the free-space isosurface. While the oscillation is still fast, the small isosurface cannot accommodate many oscillations, yielding a sizable value of the integral. Figure 2e shows that this strong interaction is sustained over a long distance if the isosurface is small. Specifically, for an isosurface with a radius of q , the real part of interaction Γ_{Re} scales as $\sin(qR)/qR$. As the isosurface radius approaches zero $q \rightarrow 0$, the range becomes infinite. Here, we use a polarization factor $\rho_{\mathbf{k}}$ based on plane waves, which, thought a simplification, is sufficient for calculating the scaling.

The size of isosurface is fixed in free space. But there are many structured photonic environments that offer smaller isosurfaces. Here, we use Weyl photonic crystals as an example to demonstrate the inverse relationship between the interaction range and the isosurface. Weyl photonic crystals [27] exhibit a conic dispersion relation in 3D space, similar to Dirac dispersion relation in two-dimensional space. The isosurface gradually reduces to a point around the apex of the conic dispersion, i.e. the Weyl point. Observation of this small isosurface suggests that we could expect long-range interactions around isolated Weyl points. Specifically, we consider a double gyroid structure described by $g(\mathbf{r}) = \sin(2\pi x/a) \cos(2\pi y/a) + \sin(2\pi y/a) \cos(2\pi z/a) + \sin(2\pi z/a) \cos(2\pi x/a)$, where a

is the lattice constant. A material with a dielectric constant $\epsilon_r = 13$ fills the regions defined by $g(\mathbf{r}) > 1.1$ and $g(\mathbf{r}) < -1.1$. Four air spheres are placed in the dielectric material as defects to break parity symmetry, but make all Weyl points present to a same frequency [28]. The unit structure is shown Fig. 3(a). The dispersion relation on the plane of $k_z = 0$ is shown in Fig. 3b with two pairs of Weyl points at the frequency $\omega_{\text{wp}} = 0.55096 c/a$. The isosurface becomes infinitesimally small at the Weyl point.

Using these isosurfaces, we numerically calculate the interaction between two TLSs placed inside the Weyl crystal. The photonic modes are simulated using MPB software package [29]. The details of the calculation are shown in the supplementary material. Figure 3c shows the interaction as a function of the inter-TLS distance for three different transition frequencies, which are also labeled by white lines in Fig. 3b. The isosurfaces have four lobes because there are four Weyl points, as shown in Fig. 3c (i-iii). As the TLSs' transition frequency approaches the Weyl points, the isosurface size decreases, causing the interaction to extend to a significantly greater range. When the transition frequency is $0.00024c/a$ away from the Weyl point (panel 'iii' in Fig. 3c), the interaction shows negligible decay even at 30 wavelengths (Fig. 3c bottom).

The decaying and oscillating patterns in these curves are attributed to a few different origins. At the largest

scale, the envelop scales as $\sin(\bar{q}R)/\bar{q}R$, where we use \bar{q} to roughly characterize the size of the subsurface (we will discuss the impact of the shape of isosurface later). The medium-range oscillation is due to the interplay of four Weyl points at the same frequency. The fastest oscillation is due to the modulation of the nonuniform field within a unit cell of the photonic crystal. The long-range interaction observed here is robust in that it does not rely on the orientation of the dipole direction or the spatial placement of TLSs (See more discussion in the supplementary material)

We can quantitatively characterize the interaction range by numerically fitting the envelope. These envelopes are shown by the dashed line in Fig. 3c. We further define a range ℓ_D as the distance when the envelop drops by to half of its maximum value. We calculate this range for TLSs at different transition frequencies near Weyl points, corresponding to different isosurface sizes. The results are shown in Fig. 3d. A clear linear relationship is demonstrated between ℓ_D and the inverse of the isosurface size $1/\bar{q}$. Because the isosurfaces are not spherical, we use $\bar{q} = \sqrt{S_\omega/4\pi}$ to define the isosurface size, where S_ω is the surface area of isosurfaces.

Thus far, we have shown that the size of the isosurface plays a critical role in the interaction range. Next, we will discuss the role of the shape of the isosurface. A spherical isosurface leads to an isotropic interaction range. On the other hand, a non-spherical isosurface generally creates an anisotropic interaction range: the interaction range depends on the direction of the inter-TLS distance vector $\hat{\mathbf{R}}$. There is a general reciprocal relationship between the interaction range and the dimension of the isosurface when projected along $\hat{\mathbf{R}}$.

Let us take the example of an ellipsoidal isosurface in anisotropic mediums. The interaction range is longer when the two TLSs are placed along the direction of the short axis of the ellipsoid $\hat{\mathbf{s}}$, than when they are along the long axis $\hat{\mathbf{l}}$. We can easily see this effect by observing the oscillation pattern of $\rho_{\mathbf{k}}e^{i\mathbf{k}\cdot\mathbf{R}}$ on an ellipsoidal isosurface as shown in Fig. 4a. When $\hat{\mathbf{R}}$ is parallel to the long axis $\hat{\mathbf{l}}$, we have many oscillations and strong cancellation of the integration. On the other hand, when $\hat{\mathbf{R}}$ is parallel to the short axis $\hat{\mathbf{s}}$, we have fewer oscillations and weaker cancellation.

To demonstrate this effect in Weyl photonic crystals, we plot the isosurface at frequency $\omega = \omega_{\text{wp}} + 0.0084c/a$, where the isosurface has a flat edge-softened rectangular geometry (Fig. 4b). We plot the integrand in Eq. (2) on the isosurface for three different \mathbf{R} . Here the magnitude of \mathbf{R} is fixed, but its direction $\hat{\mathbf{R}}$ varies from the short axis $\hat{\mathbf{s}}$ to the long axis $\hat{\mathbf{l}}$. The cancellation effect is weaker when \mathbf{R} is aligned with the short axis and stronger along the long axis. We also calculate the interaction as a function of the distance for the three directions shown in Fig. 4b. The range is conspicuously longer for TLSs placed along the short axis of the iso-

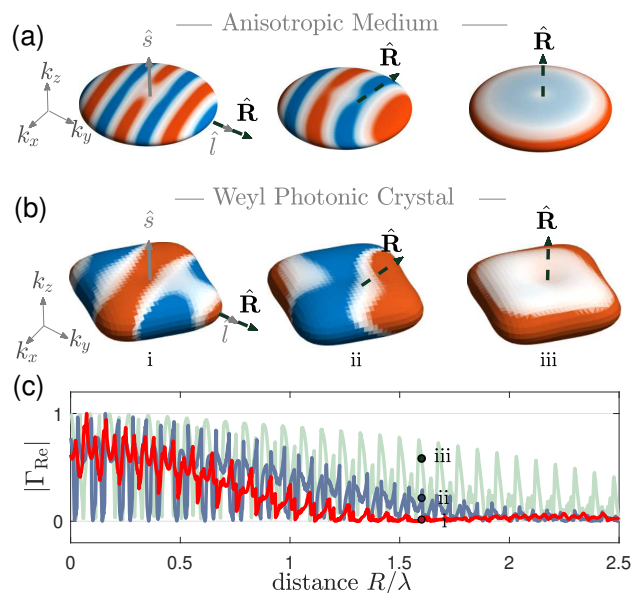


Figure 4. (a) Real part of the integrand in Eq. (2) on an elliptical isosurface with (left) $\hat{\mathbf{R}} = (0, 1, 0)$, (middle) $(0, 1, 1)/\sqrt{2}$, and (right) $(0, 0, 1)$. Unit vectors $\hat{\mathbf{s}}$ and $\hat{\mathbf{l}}$ represent short and long axis of the anisotropic isosurface. The dipole orientation is fixed as $\hat{\boldsymbol{\mu}}_{1,2} = (0, 0, 1)$. (b) Same as (a), but the isosurface is in the Weyl photonic crystal in Fig. 3a at frequency $\omega = 0.555c/a$ and the dipole orientation is fixed as $\hat{\boldsymbol{\mu}}_{1,2} = (0, 1, 0)$. (c) The absolute value of Γ_{Re} as a function of distance R . Light green, blue and dark red curves respectively correspond to $\hat{\mathbf{R}}$ in left, middle, and right cases of (b).

surface than that for the long axis as shown in Fig. 4c. In the case shown in Fig. 4, the frequency is greatly detuned from the Weyl point, and thus, the interaction range is not as long as those shown in Fig. 3.

Visual inspection of the isosurface provides a convenient tool to understand a broad class of long-range interaction phenomena. We now comment on the connection between our approach and the existing literature. The behavior of index-near-zero material [30] was explained by a long effective wavelength. Alternatively, it can also be conveniently explained by our method: the index-near-zero material also has an ultra-small isosurface. However, there is an important difference. In index-near-zero materials, the interaction range is still limited to the effective wavelength. In Weyl crystals, the interaction extends over more than hundreds of effective wavelengths. In addition to these examples, we can envision that Dirac points in 2D photonic crystals also provide small ‘isosurfaces’ (isofrequency contours) for long-range interaction [31]. Ref. [16] shows that *inside* the photonic bandgap, long tails of evanescent fields can induce long-range interaction. Here we can also see that *outside* the photonic bandgap but near the band edge, the propagating far fields have small isosurfaces, offer-

ing a different mechanism for long-range interaction. A hyperbolic material, where long-range interactions were allowed along specific directions, was treated using the Green's function method [24]. Using our graphic interpretation allows one to intuitively see that only special directions allow long-range interaction (see visualization in supplementary material).

To conclude, we show the deep connection between the long-range interaction and the isosurface in momentum space. Both size and shape of the isosurface affects the interaction range. The method introduced here provides an intuitive understanding of underlying physics that is somewhat buried in traditional treatments, and we were able to use our method to help understand several photonic systems from the existing literature. It also provides a general recipe to search for new photonic systems that support long-range interactions. As an example, we show Weyl photonic crystals as a platform to realize long-range interaction. It enables radiative interactions that extend far beyond both the vacuum and effective wavelength in 3D space for all directions. To our best knowledge, it is the first photonic system to exhibit such properties. It creates new possibilities to study collective phenomena such as superradiance and resonant energy transfer, which could lead to new applications of Weyl crystals for quantum information processing.

This work was supported by National Science Foundation (NSF) through the University of Wisconsin Materials Research Science and Engineering Center DMR-1720415. L.Y. and Z.Y. were also supported by Defense Advanced Research Projects Agency (DARPA) (DETECT program).

* zyu54@wisc.edu

- [1] M. O. Scully and A. A. Svidzinsky, *Science* **325**, 1510 (2009).
- [2] P. Solano, P. Barberis-Blostein, F. K. Fatemi, L. A. Orozco, and S. L. Rolston, *Nature communications* **8**, 1857 (2017).
- [3] Z. Meir, O. Schwartz, E. Shahmoon, D. Oron, and R. Ozeri, *Phys. Rev. Lett.* **113**, 193002 (2014).
- [4] R. M. Clegg, *Current opinion in biotechnology* **6**, 103 (1995).
- [5] F. J. Garcia-Vidal and J. Feist, *Science* **357**, 1357 (2017).
- [6] A. F. Van Loo, A. Fedorov, K. Lalumière, B. C. Sanders, A. Blais, and A. Wallraff, *Science* **342**, 1494 (2013).
- [7] G. Burkard and A. Imamoglu, *Physical Review B* **74**, 041307 (2006).
- [8] D. Petrosyan and M. Fleischhauer, *Physical review letters* **100**, 170501 (2008).
- [9] S. F. Mingaleev, Y. S. Kivshar, and R. A. Sammut, *Physical Review E* **62**, 5777 (2000).
- [10] A. Gonzalez-Tudela, D. Martin-Cano, E. Moreno, L. Martin-Moreno, C. Tejedor, and F. J. Garcia-Vidal, *Physical review letters* **106**, 020501 (2011).
- [11] E. Shahmoon and G. Kurizki, *Physical Review A* **87**, 033831 (2013).
- [12] J. D. Hood, A. Goban, A. Asenjo-Garcia, M. Lu, S.-P. Yu, D. E. Chang, and H. Kimble, *Proceedings of the National Academy of Sciences* **113**, 10507 (2016).
- [13] A. Imamog, D. D. Awschalom, G. Burkard, D. P. DiVincenzo, D. Loss, M. Sherwin, A. Small, *et al.*, *Physical review letters* **83**, 4204 (1999).
- [14] D. Maxwell, D. Szwed, D. Paredes-Barato, H. Busche, J. D. Pritchard, A. Gauguier, K. J. Weatherill, M. Jones, and C. S. Adams, *Physical review letters* **110**, 103001 (2013).
- [15] G. Kurizki, *Physical Review A* **42**, 2915 (1990).
- [16] J. S. Douglas, H. Habibian, C.-L. Hung, A. V. Gorshkov, H. J. Kimble, and D. E. Chang, *Nature Photonics* **9**, 326 (2015).
- [17] V. Notararigo, R. Passante, and L. Rizzuto, *Scientific reports* **8**, 5193 (2018).
- [18] A. Mahmoud, I. Liberal, and N. Engheta, *Optical Materials Express* **7**, 415 (2017).
- [19] I. Liberal and N. Engheta, *Proceedings of the National Academy of Sciences* **114**, 822 (2017).
- [20] I. Liberal and N. Engheta, *Physical Review A* **97**, 022309 (2018).
- [21] Y. Sato, Y. Tanaka, J. Upham, Y. Takahashi, T. Asano, and S. Noda, *Nature Photonics* **6**, 56 (2012).
- [22] F. Le Kien and A. Rauschenbeutel, *Physical Review A* **95**, 023838 (2017).
- [23] S.-A. Biehs, V. M. Menon, and G. Agarwal, *Physical Review B* **93**, 245439 (2016).
- [24] C. L. Cortes and Z. Jacob, *Nature communications* **8**, 14144 (2017).
- [25] W. D. Newman, C. L. Cortes, A. Afshar, K. Cadien, A. Meldrum, R. Fedosejevs, and Z. Jacob, *Science advances* **4**, eaar5278 (2018).
- [26] S. Bay, P. Lambropoulos, and K. Mølmer, *Physical Review A* **55**, 1485 (1997).
- [27] L. Lu, L. Fu, J. D. Joannopoulos, and M. Soljačić, *Nature photonics* **7**, 294 (2013).
- [28] L. Wang, S.-K. Jian, and H. Yao, *Physical Review A* **93**, 061801 (2016).
- [29] S. G. Johnson and J. D. Joannopoulos, *Optics express* **8**, 173 (2001).
- [30] R. Fleury and A. Alu, *Physical Review B* **87**, 201101 (2013).
- [31] A. González-Tudela and J. I. Cirac, *Physical Review A* **97**, 043831 (2018).